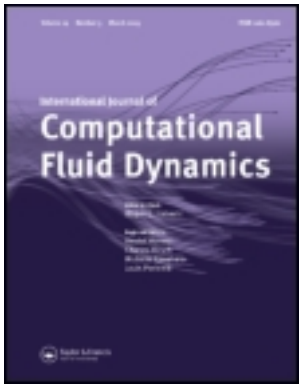

International Journal of Computational Fluid Dynamics
Publication details, including instructions for authors and subscription information:
http://www.tandfonline.com/loi/gcfd20

The Riemann problem for a hyperbolic model of two-phase flow in conservative form

D. Zeidan [a]
[a] Department of Applied Sciences, Al-Balqa Applied University, Al-Salt, Jordan

Available online: 23 Aug 2011

To cite this article: D. Zeidan (2011): The Riemann problem for a hyperbolic model of two-phase flow in conservative form, International Journal of Computational Fluid Dynamics, 25:6, 299-318

To link to this article: http://dx.doi.org/10.1080/10618562.2011.590800

International Journal of Computational Fluid Dynamics
Vol. 25, No. 6, July 2011, 299–318

Taylor & Francis
Taylor & Francis Group

The Riemann problem for a hyperbolic model of two-phase flow in conservative form

D. Zeidan*

Department of Applied Sciences, Al-Balqa Applied University, Al-Salt, Jordan

(*Received 4 January 2011; final version received 30 April 2011*)

This article is to continue the present author's work (*International Journal of Computational Fluid Dynamics* (2009) 23 (9), 623–641) on studying the structure of solutions of the Riemann problem for a system of three conservation laws governing two-phase flows. While existing solutions are limited and found quite recently for the Baer and Nunziato equations, this article presents the first instance of an exact solution of the Riemann problem for two-phase flow in gas–liquid mixture. To demonstrate the structure of the solution, we use a hyperbolic conservative model with mechanical equilibrium and without velocity equilibrium. The Riemann problem solution for the model equations comprises a set of elementary waves, rarefaction and discontinuous waves of various types. In particular, such a solution treats both the wave structure and the intermediate states of the two-phase gas–liquid mixture. The resulting exact Riemann solver is fully non-linear, direct and complete. On this basis then, we use locally the exact Riemann solver for the two-phase flow in gas–liquid mixture within the framework of finite volume upwind Godunov methods. In order to demonstrate the effectiveness and accuracy of the proposed solver, we consider a series of test problems selected from the open literature and compare the exact and numerical results by using upwind Godunov methods, showing excellent oscillation-free results in two-phase fluid flow problems.

Keywords: two-phase mixture conservation laws; hyperbolic conservative equations; Riemann problem; exact Riemann solver; Godunov upwind methods

1. Introduction

While mathematical models are a well-established tool in most of multiphase fluid flow problems and their extent and validity status as a link between theory and numerics is fairly understood, there exist considerable challenges regarding the Riemann problem for systems of partial differential equations describing multiphase flows. Such systems are usually derived by either an averaging approach or a mixture theory approach, see Ishii (1975), for example. In either approach, the resulting two-phase system is ill-posed as an initial value problem and cannot be expressed in conservation law form leading to unstable numerical methods (Stewart and Wendroff 1984). The averaging approach has served as the foundation for most subsequent mathematical and numerical work in this area. Both modelling and numerical work on two-phase flows have been investigated by many authors for decades. For a detailed presentation and description of both issues we refer the interested reader to the expository works (Stewart and Wendroff 1984, Enwald *et al*. 1996, Drew and Passman 1998, Saurel and Abgrall 1999, Gonthier and Powers 2000, Stadtke 2006, Luke and Cinnella 2007, Sachdev *et al*. 2007, Zeidan *et al*. 2007, Zeidan and Slaouti 2009, Zeidan 2011) and references therein.

Theoretical, or exact, solutions to the Riemann problem for two-phase flow equations have been developed for several two-phase flow models. Due to the complex nature of the equations describing such models, early exact solutions were limited and based on certain simplifications such as Andrianov and Warnecke (2004) solution to the Riemann problem for the Baer and Nunziato (1986) equations. This solution is classified as an indirect solution as Andrianov and Warnecke (2004) assume a solution and then they look for initial data that corresponds to the assumed solution. Schwendeman *et al*. (2006) provided the first direct Riemann solver for the same two-phase flow equations. Castro and Toro (2006), provided a direct theoretical solution for a two-phase flow equations that have a similar mathematical form to the original Baer and Nunziato equations. Another recent theoretical Riemann solver is presented by Deledicque and Papalexandris (2007) for the Baer and Nunziato equations, which is based on an initial discontinuity on the solid volume fraction. It is noted that these exact Riemann solvers were generally

*Email: dia@bau.edu.jo

ISSN 1061-8562 print/ISSN 1029-0257 online

DOI: 10.1080/10618562.2011.590800
http://www.informaworld.com

carried out on the basis of the Baer and Nunziato equations that describe a gas and solid two-phase flow. Particularly, these solvers represent the most complete and general analytical solution currently available for two phase systems. It is thus interesting to develop a solution to the Riemann problem for different classifications of two-phase flows which is the case in the current article. This article is about the Riemann problem for a recent mathematical model for a particular combination of gas–liquid two phase system in which the relative velocity between the two phases is implemented by a kinetic constitutive equation (Zeidan and Slaouti 2009). The mathematical model is a two-fluid model type (Ishii 1975) formulated in terms of parameters of state for an isentropic two-phase gas–liquid mixture. A key aspect of two-phase mixture formulation is that the system of equations is fully conservative without any conventional source terms. In addition to that, two-phase mixture formulation yields a system of equations that is hyperbolic with a complete set of eigenvalues and eigenvectors that are all real (Zeidan and Slaouti 2009). In the frame of these distinctive features, the system of equations allows the development of a direct theoretical solution of the Riemann problem to the mathematical model. Furthermore, the model is independent of the kind of numerical method employed to implement it. As a consequence, the mathematical model allows a straightforward extension and application of high-resolution finite volume methods developed for compressible gas dynamics, see for example Stadtke (2006) and Toro (2009), which make use of the hyperbolic character of the flow equations. Thus, rather than developing new numerical techniques specific to the mathematical model at hand, it is proposed to adapt finite volume methods of compressible gas dynamics. Within the context of numerical methods, the model proposed by Zeidan and Slaouti (2009) was solved by using Godunov methods of centred-type where the solution of the Riemann problem is fully numerical. It was shown that the model together with centred methods produce oscillation-free solutions for modelling discontinuous solutions in two-phase flow problems. Motivated by the previous work developed by Zeidan and Slaouti (2009), it has been recognised that a closed form solution to the Riemann problem in two-phase gas–liquid mixture can be achieved not only for the use of numerical methods but also for validating the model. The present article, therefore, adds two new aspects to two-phase flow problems. First, a procedure for the exact solution of the Riemann problem in two-phase flow with generic initial conditions is developed for the mixture formulations. Second, the approach discussed for numerical solution of the model equations is based on Godunov methods of upwind-type which employ the solution of the Riemann problem. It is important to point out, in the current article, we will not discuss the non-homogeneous part of the governing equations; a more detailed investigation for the non-homogeneous part can be found in the recent paper (Zeidan and Slaouti 2009). Within the context of the Riemann problem for the mixture, exact solution requires systematic evaluation of the solution across each characteristic field. In particular, an analysis presented by Zeidan and Slaouti (2009) has shown that the Riemann problem solution comprises a central linearly degenerate contact wave together with all other waves being genuinely non-linear. For the numerical treatment of the model equations, the Riemann problem solution is employed in the development of the Godunov first-order upwind scheme (Godunov 1959). To improve the accuracy of the scheme, the MUSCL-Hancock approach (van Leer 1979) is constructed for the data reconstruction of fluxes.

The structure of this article is as follows. Section 2 presents briefly the mathematical model for two-phase gas–liquid mixture. Section 3 explains how the exact Riemann solver for two-phase gas–liquid mixture can be derived for the flow equations. Subsequently, the Riemann problem is incorporated into upwind Godunov methods in a straightforward manner in section 4. This is followed by section 5 in which the foregoing Riemann solver and numerical methods are applied to a series of test problems. Section 6 closes the article with the conclusions.

2. A conservative hyperbolic mixture model

A hyperbolic mixture conservation laws of the one-dimensional two-phase isentropic flow with different velocities can be written as (Zeidan and Slaouti 2009)

$$\frac{\partial \mathbb{U}}{\partial t}+\frac{\partial \mathbb{F}(\mathbb{U})}{\partial x}=\mathbb{S}(\mathbb{U}). \tag{1}$$

Here t, x, $\mathbb{U}$, $\mathbb{F}$ and $\mathbb{S}$ denote the time, space coordinate, vector representing the conserved flow variables, flux and source term vectors, respectively. The vector terms are given by

$$\mathbb{U}=\begin{pmatrix}\rho\\ \rho u\\ u_r\end{pmatrix},\quad \mathbb{F}(\mathbb{U})=\begin{pmatrix}\rho u\\ \rho u^2+\rho\, c\,(1-c)\,u_r^2+P\\ uu_r+\frac{1-2c}{2}\,u_r^2+\psi(P)\end{pmatrix}$$
$$\text{and}\quad \mathbb{S}(\mathbb{U})=\begin{pmatrix}0\\ \rho g\\ \frac{\mathcal{S}^I}{\rho c(c-1)}\end{pmatrix}. \tag{2}$$

Furthermore, the notations ρ, u, u_r, P, $\psi(P)$, c, g and $\mathcal{S}^{\mathcal{I}}$ denote the mixture density, mixture velocity, relative velocity, pressure, a function that relates the two phases through the momentum equations, gas volume concentration, the gravity and the interaction between phases, respectively. The system is clearly conservative in terms of parameters of state for the two-phase gas–liquid mixture. This system is also hyperbolic and admits the following three eigenvalues up to first order in the relative velocity u_r as discussed by Zeidan and Slaouti (2009)

$$\lambda_1 = u - a_m + \mathcal{Y}u_r, \quad \lambda_2 = u + [1 - 2c - 2\mathcal{Y}]u_r \quad \text{and} \quad \lambda_3 = u + a_m + \mathcal{Y}u_r, \tag{3}$$

where a_m denotes the speed of sound of the mixture and $\mathcal{Y}$ is given by

$$\mathcal{Y} = \rho c(1 - c)\frac{\partial \psi}{\partial P}. \tag{4}$$

A detailed derivation and additional arguments justifying the present model equations and the eigenstructure analysis were performed by Zeidan and Slaouti (2009). The fields associated with λ_1 and λ_3 for the mixture are genuinely non-linear, whereas the field associated with λ_2 is neither genuinely non-linear nor linearly degenerate.

3. The Riemann problem in gas–liquid mixture

The Riemann problem for the one-dimensional two-phase gas–liquid mixture in processes without dissipation, that is no source terms, up to first order in u_r is

$$\frac{\partial \mathbb{U}}{\partial t} + \frac{\partial \mathbb{F}(\mathbb{U})}{\partial x} = 0, \quad \forall x \in \mathbb{R}, \quad t > 0, \tag{5}$$

with initial states

$$\mathbb{U}(x, t = 0) = \begin{cases} \mathbb{U}_{\mathrm{L}} = [\rho_{\mathrm{L}}, (\rho u)_{\mathrm{L}}, u_{r\mathrm{L}}], & \text{if} \quad x \le x_0, \\ \mathbb{U}_{\mathrm{R}} = [\rho_{\mathrm{R}}, (\rho u)_{\mathrm{R}}, u_{r\mathrm{R}}], & \text{if} \quad x > x_0, \end{cases} \tag{6}$$

where the subscripts L and R indicate the left and right regions, respectively, separated by a discontinuity at $x = x_0$. In general, the Riemann problem associated with the mixture consists of three distinct waves, as shown in Figure 1. The solution to the initial value problem (5) results, therefore, in the formulation of two fronts travelling in opposite direction, which can be either shock or rarefaction waves separated by a middle wave, a central discontinuity. Between the known left and right regions is the star region, which is unknown in advance and in which the mixture density, the mixture velocity and the relative velocity are determined from a Riemann solver. In addition to that, the solution in the star region consists of expressing all of the physical variables behind each wave as functions of the values of the same variables ahead of the wave and of an unknown variable behind the wave. Inspired by the exact Riemann solver described by Toro (2009) for single-phase gas dynamics and following the numerical investigations presented by Zeidan and Slaouti (2009), the solution is found after expressing all of the physical variables behind the wave as functions of the value of the mixture density at the middle wave. In other words, the problem is reduced to the search for the value of the mixture density that satisfies the jump conditions at the middle wave. It is important to note that the middle wave is neither genuinely non-linear nor linearly degenerate. As we explain further in the reset of this section, the middle wave is linearly degenerated and presents a contact wave, that is a contact discontinuity, up to first order in u_r. The properties of such wave and the Riemann problem solution will be discussed in the following sections.

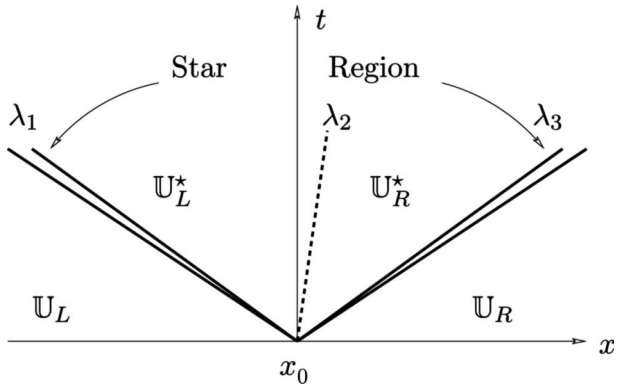

Figure 1. General solution of the Riemann problem for two-phase gas–liquid mixture of Zeidan and Slaouti (2009) in the $x-t$ plane. The Riemann problem is composed of two non-linear waves and a linear contact wave, thus resembling the structure of the Riemann problem in two-phase gas–liquid mixture. Indicated with $\mathbb{U}_{\mathrm{L}} - \mathbb{U}_{\mathrm{R}}$ are the four regions, left and right known regions and star left and star right unknown regions, into which the Riemann problem can be decomposed, each representing a different state.

3.1. Solution across waves

3.1.1. Solution across the middle wave

Before describing the solution across the waves, it is necessary to examine the solution across the middle wave λ_2. Guided by the nature of the characteristic fields of the model equations developed by Zeidan and Slaouti (2009), the second characteristic field is neither

genuinely non-linear nor linearly degenerate on $\mathbb{R}^3$. This is known as complex contact phenomena that can occur for systems of hyperbolic conservation laws (LeVeque 1992). Thus, two different cases need to be distinguished for the middle wave of the current mathematical model. The first case is a middle-shock wave while the second case is a middle-rarefaction wave. For the middle-shock wave, the Rankine–Hugoniot jump conditions for system (5) connecting the overlapping star regions either side of the wave are given by

$$S[\mathbb{U}] = [\mathbb{F}], \tag{7}$$

where for any component ξ, $[\xi] = \xi^*_{\mathrm{L}} - \xi^*_{\mathrm{R}}$, for which the star values correspond to the physical variables of the two-phase gas–liquid mixture in the star region. Then it follows easily that the following relations, after rearrangement and simplification, do not jump across the middle-shock wave up to first order in u_r

$$\rho^*_{\mathrm{L}} = \rho^*_{\mathrm{R}} = \rho^* \quad \text{and} \quad u^*_{\mathrm{L}} = u^*_{\mathrm{R}} = u^* = S, \tag{8}$$

while only the relative velocity u_r changes discontinuously so that

$$u^*_{r\mathrm{L}} \neq u^*_{r\mathrm{R}}. \tag{9}$$

Moving to the middle-rarefaction wave, a straightforward application of the generalised Riemann invariants across the middle-rarefaction wave yields

$$\frac{d\rho}{-2\rho c(1-c)u_r} = \frac{du}{0} = \frac{du_r}{1}, \tag{10}$$

which gives

$$u = \text{constant} \quad \text{and} \quad u_r^2 + \int^{\rho} \frac{d\rho}{\rho c(1-c)} = \text{constant}, \tag{11}$$

which also gives rise to the following relations up to first order in u_r

$$\rho^*_{\mathrm{L}} = \rho^*_{\mathrm{R}} = \rho^*, \quad u^*_{\mathrm{L}} = u^*_{\mathrm{R}} = u^* = S \quad \text{and} \quad u^*_{rL} \neq u^*_{rR}. \tag{12}$$

In view of the ease with which the relations (8), (9) and (12) can be specified in this way and for the purpose of this article, it is sufficient to treat the second characteristic field as a contact wave up to first order in u_r for the mixture propagating with a velocity S. Therefore, from now on we will deal with the middle wave as a contact wave across which the mixture density and the mixture velocity are constants while the relative velocity jumps discontinuously.

3.1.2. Solution across shock waves

Consider a shock wave propagating with a velocity S across which ρ, u and u_r are discontinuous. Then, the solutions of Equation (5) connecting the given left states, $\mathbb{U}_L$, and the given right states, $\mathbb{U}_R$, to the star region are found by applying the Rankine–Hugoniot jump conditions. In this case, Rankine–Hugoniot jump conditions follow from Equation (5) as

$$\pm S_k(\rho^* - \rho_k) = \pm(\rho^* u^* - \rho_k u_k), \tag{13}$$

$$\pm S_k(\rho^* u^* - \rho_k u_k) = \pm(\rho^* u^{2*} - \rho_k u_k^2 + P^* - P_k) + [\rho c(1-c)u_r^2], \tag{14}$$

$$\pm S_k(u^*_{rk} - u_{rk}) = \pm(u^* u^*_{rk} - u u_{rk} + \psi(P^*) - \psi(P_k)) + \left[\frac{1-2c}{2} u_r^2\right], \tag{15}$$

where the minus is in case of $k = \mathrm{L}$ and the plus is for $k = \mathrm{R}$. After a number of algebraic manipulations, Equations (13) and (14) give

$$u^* = u_k \pm F_k(\rho^*, \mathbb{U}_k), \tag{16}$$

with

$$F_k(\rho^*, \mathbb{U}_k) = (\rho^* - \rho_k)\left[\frac{\mathcal{B}_k}{\mathcal{A}_k(\rho^* - \rho_k)}\right]^{\frac{1}{2}},$$

and

$$\mathcal{A}_k = \frac{\rho^*}{\rho_k}, \ \mathcal{B}_k = \frac{P^* - P_k}{\rho_k^2}.$$

Next, combining Equation (13) with (15) leads to the value of the relative velocity in the star region

$$u^*_{rk} = \mathcal{A}_k u_{rk} \pm (\psi(P^*) - \psi(P_k))\left[\frac{\mathcal{A}_k}{\rho_k^2}\frac{\rho^* - \rho_k}{\mathcal{B}_k}\right]^{\frac{1}{2}}, \tag{17}$$

bearing in mind that only the relative velocity changes across the contact discontinuity, while the mixture density and mixture velocity remain constant in the star region as noted previously.

3.1.3. Solution across rarefaction waves

Applying the Riemann invariants across the mixture left and right rarefactions waves gives

$$\frac{d\rho}{\rho a_m} = \frac{du}{\pm 1 + \mathcal{Y}\frac{u_r}{a_m}} = \frac{du_r}{\pm\rho\frac{\partial\psi}{\partial P} + \rho\frac{u_r}{a_m}\frac{\partial\psi}{\partial P}\left(1 - 2c - \mathcal{Y} + \frac{1}{\rho}\frac{\partial P}{\partial\psi}\right)}. \tag{18}$$

Manipulation of these quantities leads to

$$u \pm \frac{-2}{\gamma - 1} a_m = \text{constant}, \tag{19}$$

$$u_r \pm \frac{-2}{\gamma - 1}\frac{\rho}{\rho_2} a_m \pm \frac{2}{\gamma + 1}\frac{\rho}{\rho_1} a_m = \text{constant}. \tag{20}$$

After a number of tedious algebraic manipulations Equation (19) gives

$$u^* = u_k \pm F_k(\rho^*, \mathbb{U}_k), \tag{21}$$

with

$$F_k = \frac{2}{\gamma - 1}\, a_{mk}\left[\left(\frac{\rho^*}{\rho_k}\right)^{\frac{\gamma-1}{2}} - 1\right].$$

Finally, Equation (20) provides us with the relative velocity in the star region

$$\begin{aligned} u^*_{rk} = u_{rk} \pm \frac{2}{\gamma + 1}\left\{\frac{\gamma + 1}{\gamma - 1}\frac{\rho^*}{\rho_2}\left[\left(\frac{\rho^*}{\rho_k}\right)^{\frac{\gamma-1}{2}} - 1\right]\right. \\ \left. + \frac{\rho^*}{\rho_1}\left[\frac{\rho_k}{\rho^*} - \left(\frac{\rho^*}{\rho_k}\right)^{\frac{\gamma-1}{2}}\right]\right\} a_{mk}, \end{aligned} \tag{22}$$

with the minus is in case of $k = \mathrm{L}$ and the plus is for $k = \mathrm{R}$. It should be observed that only the relative velocity u_r jumps across the contact while the mixture density and mixture velocity remain constant across the star region, as the case for shock waves. It is also clear that the given states $\mathbb{U}_\mathrm{L}$ and $\mathbb{U}_\mathrm{R}$ are connected to the star region by Equations (21) and (22).

3.2. Solution within the star region

The solution within the star region is found from the relations valid across the left and right waves connecting the flow variables, ρ^*, u^* and u^*_{rk} to the known left states and to the known right states. Equations (16) and (21) lead to a non-linear algebraic equation for ρ^* as

$$F(\rho^*, \mathbb{U}_\mathrm{L}, \mathbb{U}_\mathrm{R}) \equiv F_\mathrm{L}(\rho^*, \mathbb{U}_\mathrm{L}) + F_\mathrm{R}(\rho^*, \mathbb{U}_\mathrm{R}) + \Delta u = 0,$$
$$\Delta u \equiv u_\mathrm{R} - u_\mathrm{L},$$

where the functions F_L and F_R

$$F_k(\rho^*, \mathbb{U}k) = \begin{cases} (\rho^* - \rho_k)\left[\frac{\mathcal{B}_k}{\mathcal{A}_k(\rho^* - \rho_k)}\right]^{\frac{1}{2}} & \text{if} \quad \rho^* > \rho_k \ \text{(shock)}, \\ \frac{2}{\gamma - 1}\left[\left(\frac{\rho^*}{\rho_k}\right)^{\frac{\gamma-1}{2}} - 1\right] a_{mk} & \text{if} \quad \rho^* \le \rho_k \ \text{(rarefaction)}. \end{cases} \tag{24}$$

Since there is no general closed form solution to Equation (23), the exact solution is sought numerically by a Newton–Raphson iteration scheme

$$(\rho^*)^{(i+1)} = (\rho^*)^{(i)} - \frac{F(\rho^*)^i}{F'(\rho^*)^i}, \tag{25}$$

where the superscript indicates the results at the $(i)^{\text{th}}$ or $(i + 1)^{\text{th}}$ iteration and the prime represents the derivative with respect to ρ^* given by

$$F'_k = \begin{cases} \frac{1}{2\rho^*}\left[\frac{\rho_k}{\rho^* - \rho_k} + \frac{\gamma(\rho^*)^\gamma}{(\rho^*)^\gamma - \rho_k^\gamma}\right] F_k \ \text{if} \ \rho^* > \rho_k \quad \text{(shock)}, \\ \frac{a_{mk}}{\rho^*}\left[\left(\frac{\rho^*}{\rho_k}\right)^{\frac{\gamma-1}{2}}\right] \qquad \text{if} \ \rho^* \le \rho_k \quad \text{(rarefaction)}. \end{cases} \tag{26}$$

Furthermore, the iteration scheme starts with an initial guess ρ^*_0 and continues until the change in ρ^* is smaller than a prescribed tolerance.

Once the mixture density ρ is known through the star region, the mixture velocity can be evaluated as

$$u^* = \frac{1}{2}(u_{_L} + u_{_R}) + \frac{1}{2}[F_\mathrm{R}(\rho^*, {}_{U_R}) - F_\mathrm{L}(\rho^*, {}_{U_L})]. \tag{27}$$

Finally, after determining ρ^* and u^*, the value of u^*_{rk} can be calculated from the relations across the shocks, Equation (17), and the rarefactions, Equation (22), as explained in the previous section.

3.3. Solution within the wave structure

The final step in solving the Riemann problem for the mathematical model is to find the solution within the complete wave structure. Such a structure expresses shocks across the left and right waves associated with λ_1 and λ_3 for $\rho^* > \rho_k$ with the following speeds

$$S_k = u_k \pm \left[\frac{\rho^*}{\rho_k}\frac{P^* - P_k}{\rho^* - \rho_k}\right]^{\frac{1}{2}}, \tag{28}$$

where the plus is for $k = \mathrm{R}$ and the minus is the case of $k = \mathrm{L}$.

Similarly, the structure is a rarefaction waves for the left and right waves associated with λ_1 and λ_3 for $\rho^* \le \rho_k$ with speeds

$$S_{Hk} = u_k \pm a_{mk} + \mathcal{Y}\, u_{rk} \quad \text{and} \quad S_{Tk} = u^* \pm a^*_m + \mathcal{Y}^* u^*_{rk}, \tag{29}$$

where S_{Hk} and S_{Tk} are the speeds of the head and tail, respectively, of the rarefaction waves. In this case it is necessary to find the solution for the Riemann problem within the rarefaction waves. Using the generalised Riemann invariants along the characteristic that joins

the origin (0, 0) and a generic point $\hat{y}(x,t)$ inside the wave

$$\frac{dx}{dt} = u \pm a_m + \mathcal{Y}\, u_r = \frac{x}{t}, \tag{30}$$

leads to the solution inside the rarefaction fans for the mixture density as

$$\rho_k^{\text{Fan}} = \rho_k \left[\frac{2}{\gamma+1} \pm \frac{1}{a_{mk}} \left(\frac{x}{t} - u_k \right) \frac{\gamma-1}{\gamma+1} + \frac{\gamma-1}{\gamma+1} \frac{\mathcal{Y}_k^{\text{Fan}}}{a_{mk}} u_{rk}^{\text{Fan}} \right]^{\frac{2}{\gamma-1}}, \tag{31}$$

while the mixture velocity as

$$u_k^{\text{Fan}} = \frac{2}{\gamma+1} \left[\frac{x}{t} + \frac{\gamma-1}{2}\, u_k \pm (-a_{mk}) - \mathcal{Y}_k^{\text{Fan}} u_{rk}^{\text{Fan}} \right], \tag{32}$$

and the relative velocity between the two phases as

$$u_{rk}^{\text{Fan}} = u_{rk} \pm \frac{2}{\gamma+1} \left\{ \frac{\gamma+1}{\gamma-1} \frac{\rho_k^{\text{Fan}}}{\rho_2} \left[\left(\frac{\rho_k^{\text{Fan}}}{\rho_k} \right)^{\frac{\gamma-1}{2}} - 1 \right] + \frac{\rho_k^{\text{Fan}}}{\rho_1} \left[\frac{\rho_k}{\rho_k^{\text{Fan}}} - \left(\frac{\rho_k^{\text{Fan}}}{\rho_k} \right)^{\frac{\gamma-1}{2}} \right] \right\} a_{mk}. \tag{33}$$

It is clear that Equations (31–33) are non-linear. The solution, therefore, inside both the left and right rarefaction fans need to be found iteratively. This can be done once the solution for the mixture density ρ^* is found as described in the previous section. The solution in this case is found first for the mixture density ρ_k^{Fan} by substituting Equation (33) into Equation (31) and then using Newton–Raphson iteration scheme. Once the solution for ρ_k^{Fan} is known, the solution for the mixture velocity u_k^{Fan} and the relative velocity u_{rk}^{Fan} follow directly using Equations (32) and (33).

4. Numerical approach

The methodology for using the numerical approaches to solve numerically system (1) is based on finite volume Godunov methods of upwind-type which requires solutions of the Riemann problem of section 3. These methods are implemented on the basis of an extension of an advanced conservative and explicit finite volume approaches defined as

$$\mathbb{U}_i^{n+1} = \mathbb{U}_i^n - \frac{\Delta t}{\Delta x} \left[\mathbb{F}_{i+\frac{1}{2}} - \mathbb{F}_{i-\frac{1}{2}} \right] + \Delta t \mathbb{S}_i, \tag{34}$$

where the superscript n represents the time level, subscript i is the cell index, and Δt and Δx are respectively the time step and cell size, $\mathbb{F}_{i\pm12}$ are the fluxes at the interfaces of cell i, and $\mathbb{S}_i$ are source terms. Since we are primarily interested in the Riemann problem for the model at hand, we can take $\mathbb{S}_i = 0$. An upwind scheme is the Godunov first-order accurate scheme with intercell fluxes given by

$$\mathbb{F}_{i\pm\frac{1}{2}} = \mathbb{F}(\mathbb{U}_{i\pm\frac{1}{2}}(0)). \tag{35}$$

Here $\mathbb{U}_{i\pm12}(0)$ is the exact solution of the local Riemann problem at cell interface positions $i \pm 12$ evaluated at $\frac{x}{t} = 0$ in one dimension with initial states given by Equation (6). The Godunov first-order accurate scheme can be improved and extended to second and higher order upwind methods such as the MUSCL-Hancock scheme and the WAF scheme, see Toro (2009) for an overall description of different high order numerical methods.

Since the aim of this article is on the demonstration of Riemann problem of the proposed hyperbolic conservative model (1), the MUSCL-Hancock scheme is employed for the solution of the model equations. The MUSCL-Hancock approach has three steps to implement (Toro 2009). The first step is the data reconstruction by piecewise linear functions in every cell i

$$\mathbb{U}_i(x) = \mathbb{U}_i^n + (x - x_i) \frac{\Delta_i}{\Delta x}, \tag{36}$$

where Δ_i is a limited slope to produce oscillation-free solutions by using the total variation diminishing (TVD) constraints among the various slope limiter functions (Toro 2009). The boundary extrapolated values are given by

$$\mathbb{U}_i^L = \mathbb{U}_i^n - \frac{1}{2}\Delta_i \quad \text{and} \quad \mathbb{U}_i^R = \mathbb{U}_i^n + \frac{1}{2}\Delta_i. \tag{37}$$

These boundary extrapolated values are then evolved in time by half a time step as

$$(\mathbb{U}_i^{L,R})^{\text{New}} = \mathbb{U}_i^{L,R} + \frac{1}{2}\frac{\Delta t}{\Delta x}[\mathbb{F}(\mathbb{U}_i^L) - \mathbb{F}(\mathbb{U}_i^R)], \tag{38}$$

which is a linear combinations of the conserved variables and the fluxes. Finally, the numerical fluxes are computed using the solution of the Riemann problems with the evolved data $(\mathbb{U}_i^{L,R})^{\text{New}}$ as

$$\mathbb{F}_{i\pm\frac{1}{2}} = \mathbb{F}(\mathbb{U}_{i\pm\frac{1}{2}}(0)), \tag{39}$$

which is the Godunov first-order upwind scheme.

5. Numerical simulations

The purposeof this article is to establish a typical theoretical solution for the Riemann problem for a hyperbolic model of two-phase mixture flow in conservative form. Such a model has been validated by Zeidan and Slaouti (2009) with other two-phase flow models of different type for homogeneous and non-homogeneous parts of the equations. The primary interest of this article therefore is only in the Riemann problem, the homogeneous part of the model as indicated previously.

In the present section, comparisons are given between the exact and numerical solutions to a series of standard test cases some of which are well documented in the literature while the rest are new to the literature. The main purpose is to check the validity of the model, the Riemann solver and the numerical methods. The series of test cases include two parts. In the first part, no-slip law, that is $u_r = 0$, test cases are considered which consist of a pure rarefaction, shock-waves propagation within an air–water mixture, rarefaction-waves propagation within an air–water mixture and a sonic rarefaction. The second part deals with slip laws and conditions, that is $u_r \neq 0$, test cases and includes the Zuber-Findlay law, the dispersed law, left shock and right rarefaction waves and left rarefaction and right rarefaction waves. In all the following test cases, the initial value problems are solved in the one-dimensional domain $[-10, 10]$. The discontinuity between the two initial states, Equation (6), is located at $x = x_0 = 0$. Transmissive boundary conditions with a CFL stability coefficient of 0.9 together with the SUPERBEE limiter are used throughout the numerical methods. For a detailed treatment of SUPERBEE limiter and other available limiter functions, refer to Toro (2009). All the numerical results presented in Figures 2(a)–17(b) are carried out on a grid of 100 cells for two different upwind Godunov methods, namely the Godunov first-order scheme and the MUSCL-Hancock scheme using the exact Riemann solver of section 3. Figures 2(a)–17(b) display the exact solutions and the numerical

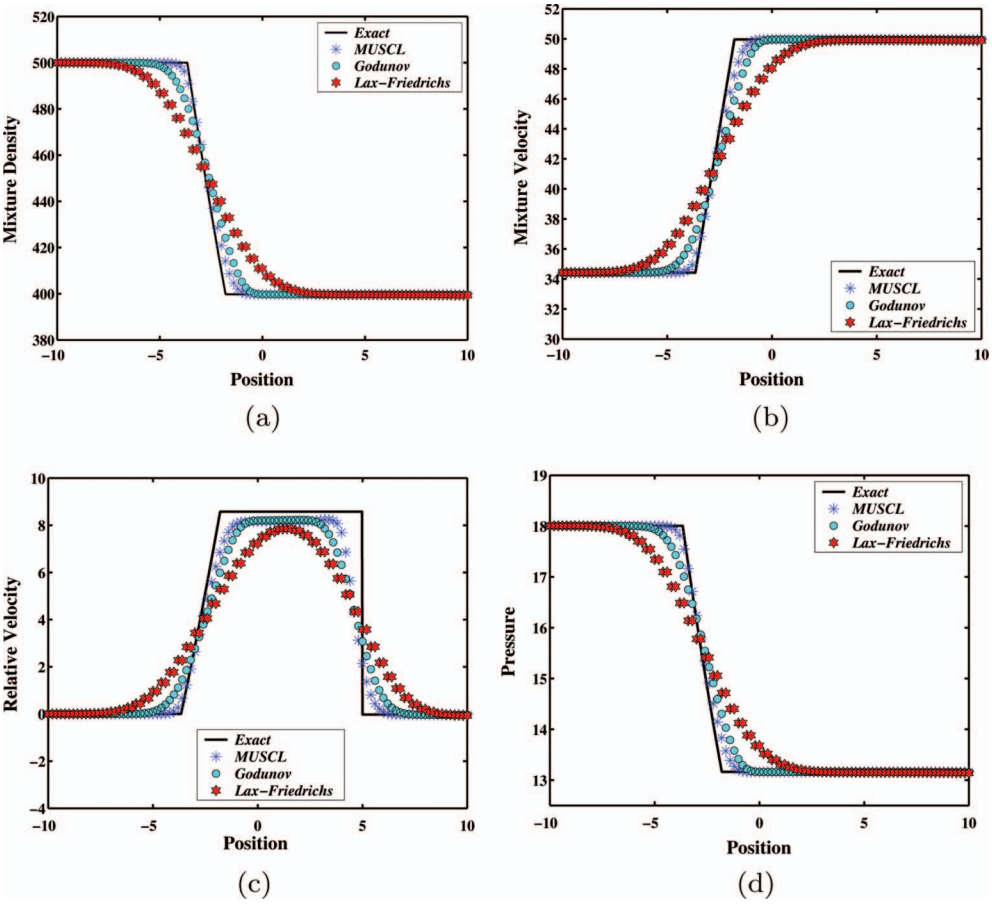

Figure 2. Comparison between exact (solid line) and numerical (symbols) solutions of the pure rarefaction test case of (Baudin *et al.* 2005a) at a time $t = 0.1$. Top left and right panels display the mixture density (kg m^{-3}) and mixture velocity (m s^{-1}), respectively while the bottom left and right panels show the relative velocity (m s^{-1}) and pressure (Pa), respectively.

results for all these tests. The different symbols in each plot refer to the different numerical methods while the solid lines correspond to the exact Riemann solver. In all test cases, as we shall see latter, we compare both the theoretical solutions and the numerical results with the Lax-Friedrichs scheme. It is useful to note that the Lax-Friedrichs scheme is a basic numerical scheme and known as a dissipative scheme more than any other scheme, see Toro (2009) for example. It is also important to note that this scheme is characterised by pairing cell values with coarse grid. Finally, we refer the reader to the web version of this article for interpretation of the waves to colour in all the figures legend throughout.

5.1. *No-slip law*

The two-phase gas–liquid mixture model with the proposed Riemann solver is first verified with no slip law, $u_r = 0$, involving four Riemann problems.

5.1.1. *Pure rarefaction*

This test case was proposed by Baudin *et al*. (2005a) and validated by Baudin *et al*. (2005b) and Munkejord *et al*. (2006) with the following initial data

$$(\rho, u, u_r)_{\mathrm{L}} = (500\ \mathrm{kg/m^3},\ 34.4233\ \mathrm{m/s},\ 0\ \mathrm{m/s}),$$
$$(\rho, u, u_r)_{\mathrm{R}} = (400\ \mathrm{kg/m^3},\ 50\ \mathrm{m/s},\ 0\ \mathrm{m/s}).$$

This test case is designed to produce a left rarefaction wave only through the wave structure. In other words, the two-phase gas–liquid mixture wave pattern consists of a pure left rarefaction wave associated with the left eigenvalue of the model equations as shown in Figure 2(a)–(d). Figure 2(a)–(d) shows the numerical results and the exact solution of the mixture density, mixture velocity, relative velocity and pressure at a time $t = 0.1$. The results show one left propagating rarefaction wave for all the flow variables, similar to those obtained by Baudin *et al*. (2005a), except for the relative velocity profile which is not displayed by Baudin *et al*. (2005a). The relative velocity behaviour shows a left propagating rarefaction wave and a strong right propagating shock wave. Between the left rarefaction and right shock waves is the star region with constant relative velocity between the two phases across the contact discontinuity. This is a physical effect that is not taken into consideration by Baudin *et al*. (2005a). Furthermore, the model presented by Baudin *et al*. (2005a) is the drift flux model which does not involve an equation for the relative velocity between the two phases while it is taken into consideration in the current model. The exact solution of the Riemann problem was computed by using the Riemann solver described in section 3. Clearly, all the numerical results are in excellent agreement with the exact solution. Further, it is concluded that upwind Riemann solver-based methods significantly improve the efficiency and the accuracy of the solution. Additionally, one notes that the star region of the relative velocity, see Figure 2(c), differs slightly between the numerical results and the exact solution. This is caused by the second order of the relative velocity, u_r^2, appearing in the flux functions (2) where the exact solution is constructed up to first order in u_r as mentioned previously. In order to obtain a deeper insight into the role of the relative velocity effect on the exact and numerical solutions, we perform a grid convergence study for the relative velocity profile using the Godunov first-order scheme and the Lax-Friedrichs scheme for gradually finer grids (a coarse grid of 100 cells, a medium grid of 500 cells and a fine grid of 1000 cells, as grids of a larger number of cells were checked to produce no further improvement) as shown in Figure 3(a,b). We chose to investigate the relative velocity because of its particular interest in the present study. From the plots, one can see that the wave structure takes finer and finer behaviour as the number of cells is increased for computations but can not converge to the exact solution. This gives us confidence that the difference between the numerical results and the exact solutions provided in the star region is caused by the order of the relative velocity as indicated previously. Finally, this test case shows the possibility of solving the simplest Riemann problem with no-slip configuration for the two-phase gas–liquid mixture.

5.1.2. *Shock-waves propagation within an air–water mixture*

This test, reported by Zeidan and Slaouti (2009), consists of two symmetric shock waves for the two-phase gas–liquid mixture. The initial conditions for this test case are

$$(\rho, u, u_r)_{\mathrm{L}} = (0.9\ \mathrm{kg/m^3},\ \ 0.5\ \mathrm{m/s},\ 0\ \mathrm{m/s}),$$
$$(\rho, u, u_r)_{\mathrm{R}} = (0.9\ \mathrm{kg/m^3}, -0.5\ \mathrm{m/s},\ 0\ \mathrm{m/s}).$$

Exact and numerical results at a time $t = 0.025$ are displayed in Figure 4(a)–(d). These results are obtained using the exact solver of section 3, the Godunov first-order scheme and the second-order MUSCL-Hancock scheme of section 4. Figure 4(a)–(d) shows the exact solution and the numerical results for the relative velocity, mixture velocity, mixture density and gas velocity. Excellent agreement between the exact and numerical solutions is achieved as displayed in Figure 4(a)–(d). The results are oscillation-free for all

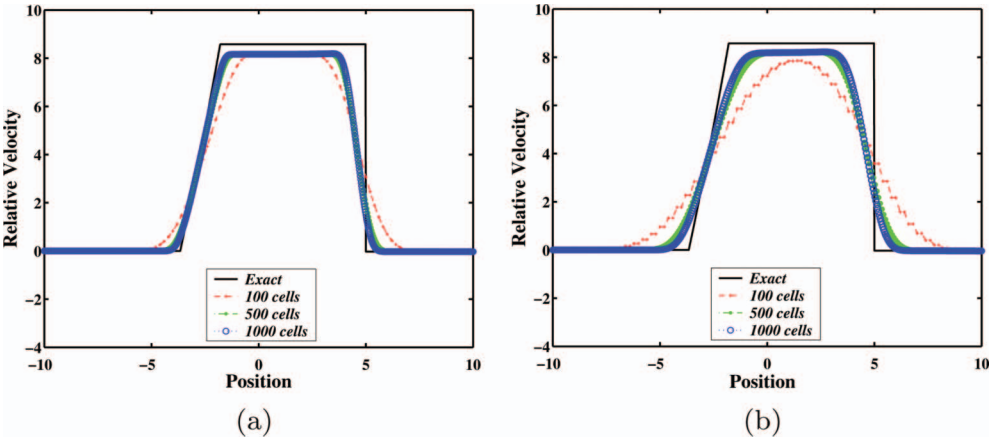

Figure 3. Grid convergence study for the pure rarefaction test case of (Baudin *et al.* 2005a). Results for the relative velocity (m s^{-1}) profile: computed (line symbols) and exact (solid line) at a time $t = 0.1$ with CFL $= 0.9$. The left panel, (a), shows results for the Godunov first-order scheme while the right panel, (b), refers to the Lax-Friedrichs scheme results, respectively.

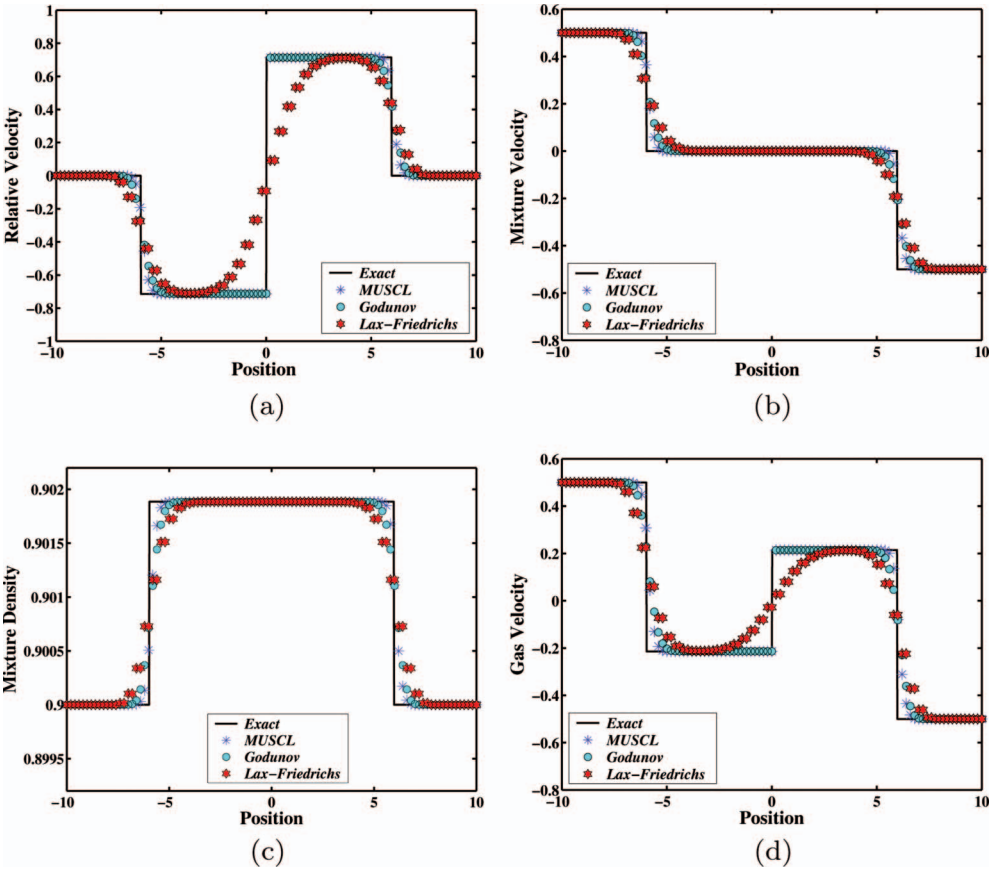

Figure 4. Comparison of exact and numerical solutions of the shock-waves propagation within an air–water mixture of Zeidan and Slaouti (2009) at a time $t = 0.025$. Symbols correspond to the numerical solution of the model equations while the exact solution is shown with solid lines. From left to right, the top panels show the relative velocity (m s^{-1}) and mixture velocity (m s^{-1}), whereas in the bottom panels display the mixture density (kg m^{-3}) and gas velocity (m s^{-1}).

variables and similar to those presented by Zeidan and Slaouti (2009). Further, upwind Riemann solver-based Godunov methods behaves much better than centred Godunov methods presented by Zeidan and Slaouti (2009). As displayed in Figure 4(a)–(d), the middle wave behaves as a contact discontinuity where the

relative velocity and gas velocity change discontinuously across eigenvalue λ_2. The plots in Figure 5(a,b) display the relative velocity profile using the Godunov first-order scheme and the Lax-Friedrichs scheme at a time $t = 0.025$ for gradually finer grids, and these give a clear indication of the convergence behaviour of the developed wave structure. This test case demonstrates that both the exact and numerical solutions with no-slip configuration can represent two symmetric shock waves without introducing any spurious oscillations.

5.1.3. *Rarefaction-waves propagation within an air–water mixture*

This test case is a particular version of the one presented by Zeidan and Slaouti (2009). The initial conditions used in the calculations are

$$(\rho, u, u_r)_{\mathrm{L}} = (800\ \mathrm{kg/m^3}, -100\ \mathrm{m/s},\ 0\ \mathrm{m/s}),$$
$$(\rho, u, u_r)_{\mathrm{R}} = (800\ \mathrm{kg/m^3},\ \ 100\ \mathrm{m/s},\ 0\ \mathrm{m/s}),$$

and the results at a time $t = 0.007$ are presented in Figure 6(a)–(d).

The two-phase gas–liquid mixture consists of two symmetric rarefaction waves and a trivial contact wave. Figure 6(a)–(d) displays the structure of the relative velocity, mixture density, gas density and liquid velocity. The results show that only the relative velocity and the liquid phase velocity profiles change discontinuously across the contact wave. Also, the results are oscillation-free and excellent agreement is found between the exact and numerical solutions. In particular, the computed exact and numerical results predict sharper features of the rarefaction waves than those by Zeidan and Slaouti (2009) because of the employed Riemann problem-based strategy. It is also interesting to note that the star region in the relative velocity and liquid phase velocity profiles differ slightly between the exact and numerical solutions. As has been observed earlier, this is due to the first and second order in u_r used within the exact Riemann solver and the numerical methods. This is clearly demonstrated in Figure 7(a,b) through grid convergence study using the Godunov first-order scheme and the Lax-Friedrichs scheme.

5.1.4. *Sonic rarefaction*

This test is designed to examine the ability of the exact Riemann solver and to estimate the performance and the accuracy of the Godunov first-order scheme and the second-order MUSCL-Hancock scheme. The initial conditions for this Riemann problem are defined as

$$(\rho, u, u_r)_{\mathrm{L}} = (1000\ \mathrm{kg/m^3},\ 4\ \mathrm{m/s},\ 0\ \mathrm{m/s}),$$
$$(\rho, u, u_r)_{\mathrm{R}} = (400\ \mathrm{kg/m^3},\ \ 3\ \mathrm{m/s},\ 0\ \mathrm{m/s}).$$

These conditions are chosen to produce for the gas–liquid mixture a sonic, or critical, left rarefaction wave, a right propagating contact discontinuity and a strong right propagating shock wave. A distinct feature of this test case is that the left rarefaction is sonic, that is, the eigenvalue $\lambda_1 = u - a_m + \mathcal{Y} u_r$ changes from a negative value to a positive value as the wave crossed from left to right. In Figure 8(a)–(d), the exact solution and the numerical results are displayed at a time $t = 1$ for different state profiles. The exact solution of the Riemann problem was calculated by the exact Riemann solver of section 3. As shown in the figure the

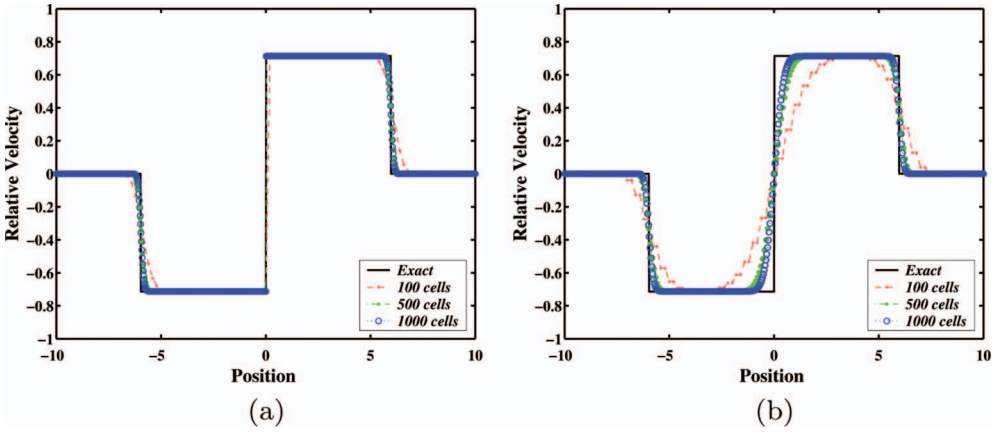

Figure 5. Grid convergence study for the shock-waves propagation within an air–water mixture of Zeidan and Slaouti (2009). Results for the relative velocity (m s^{-1}) profile: computed (line with circles, line with points and line with plus signs, respectively) and exact (solid line) at a time $t = 0.025$ with CFL = 0.9. (a) The Godunov first-order scheme resolutions. (b) The Lax-Friedrichs scheme resolutions.

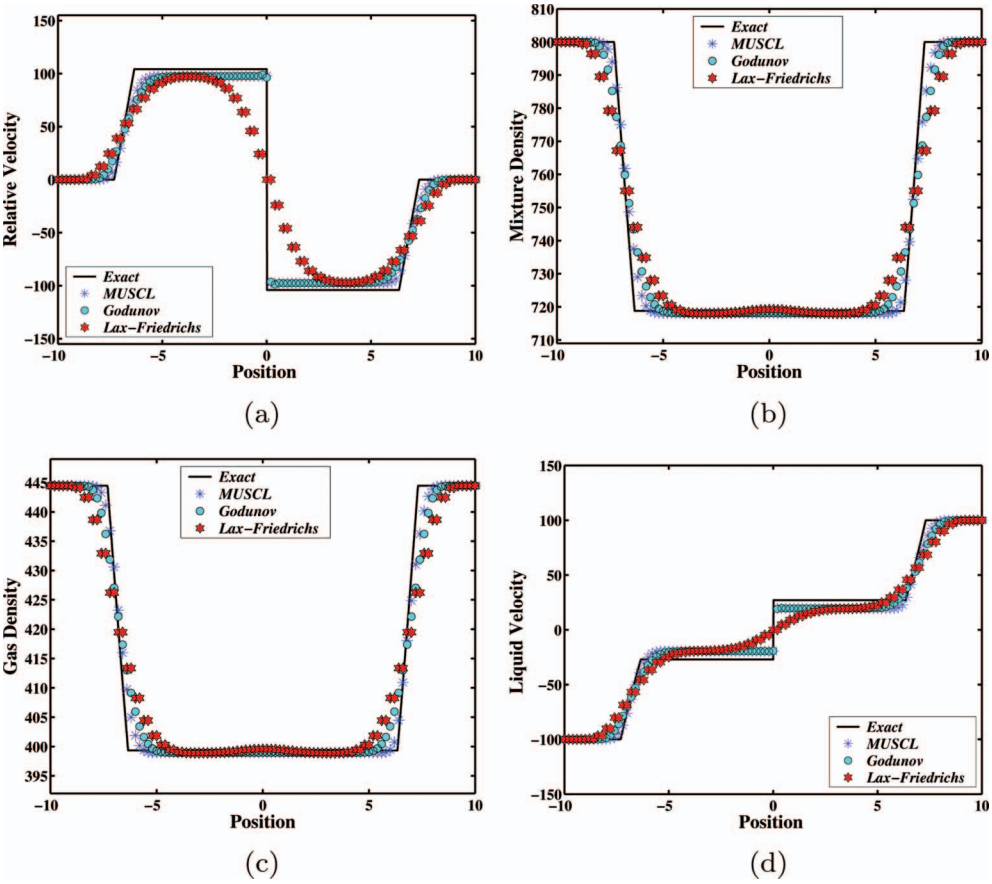

Figure 6. Comparison of exact (solid line) and numerical (symbols) solutions of the rarefaction-waves propagation within an air–water mixture of (Zeidan and Slaouti 2009) at a time $t = 0.007$. Top panel: relative velocity (m s^{-1}) and mixture density (kg m^{-3}). Bottom panel: gas density (kg m^{-3}) and liquid velocity (m s^{-1}).

numerical results are in excellent agreement with the exact solution. Further, the numerical results are free of spurious oscillations associated with the rarefaction and shock waves or across the contact wave. As one can see, the relative velocity experience jumps across the contact wave associated with the eigenvalue λ_2. Also, in the relative velocity profile one can note the difference in the star region between the exact solution and numerical results. This is related to the effect of the first and second order in u_r used within both the exact Riemann solver and the numerical methods. A more quantitative view of the solutions can be seen in Figure 9(a,b). In this figure, we show the behaviour of the relative velocity profile provided by using the first-order numerical methods for various grid resolutions. As expected, the curves of the solutions at finer resolution (shown in blue) cannot approach the exact solution.

The plots shown here and in the previous test cases provide strong evidence that these differences between the exact and numerical solutions are related to the relative velocity, u_r, order for the no slip part.

5.2. *Slip laws and conditions*

The aim of this part is to check the capability of the model, the Riemann solver and the chosen numerical methods to describe the Riemann problem in gas–liquid mixture with slip configuration.

5.2.1. *Zuber-Findlay law*

This test case was proposed by Baudin *et al.* (2005a). It consists of the following Zuber-Findlay hydrodynamic law (Zuber and Findlay 1965)

$$u_r = \frac{(c_0 - 1)u + c_1}{c_0[(1-c)\alpha - c(1-\alpha)] - (1-c)}, \qquad (40)$$

with $c_0 = 1.07$ and $c_1 = 0.2162$ m/s. The initial conditions for this Riemann problem are given by (Baudin *et al.* 2005a).

$$\rho_L = 453.197, \quad u_L = 24.8074 \quad \text{and}$$
$$\rho_R = 454.915, \quad u_R = 1.7461.$$

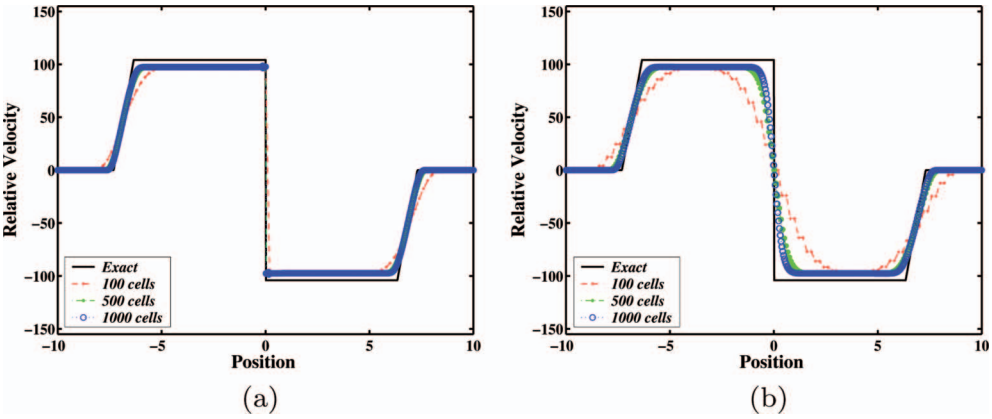

Figure 7. Grid convergence study for the rarefaction-waves propagation within an air–water mixture of (Zeidan and Slaouti 2009). Results for the relative velocity (m s^{-1}) profile: computed (line symbols) and exact (solid line) at a time $t = 0.007$ with CFL = 0.9. (a) The Godunov first-order scheme resolutions. (b) The Lax-Friedrichs scheme resolutions.

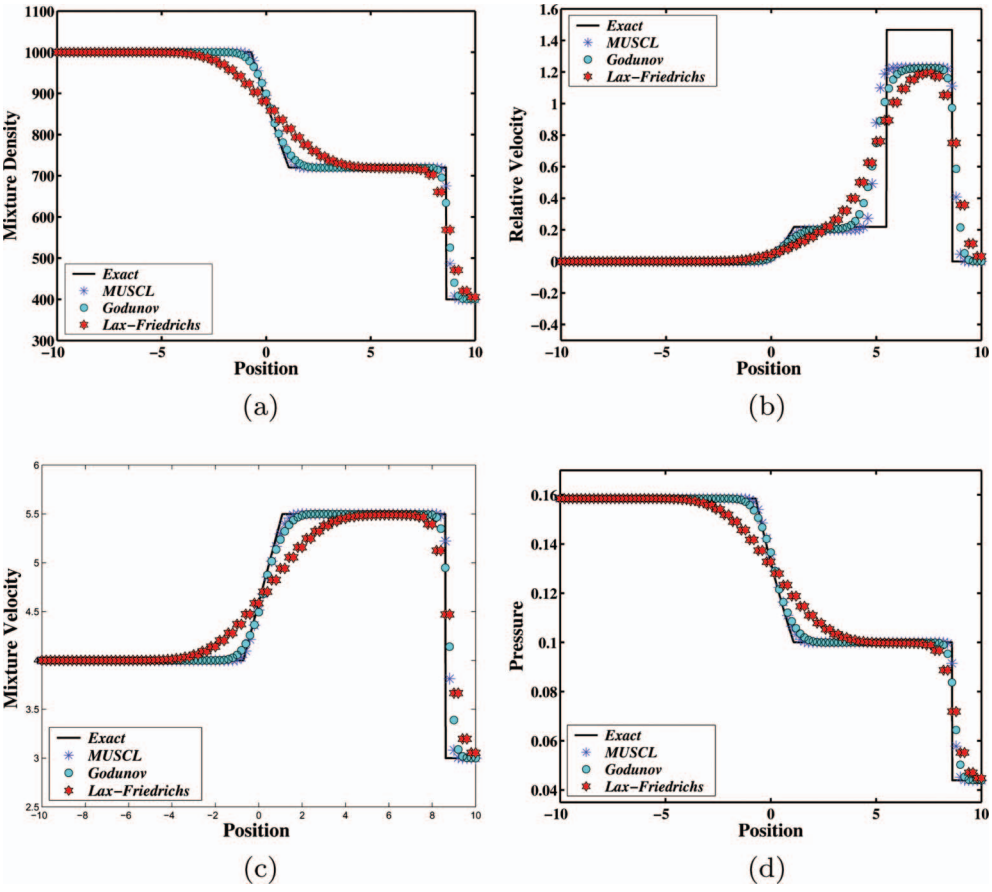

Figure 8. Comparison of exact (solid line) and numerical (symbols) solutions of sonic rarefaction test case at a time $t = 1$. The solution is composed of a right shock wave, a right travelling contact discontinuity and a left sonic rarefaction wave. Note the correct resolution of the sonic point provided by the numerical methods. The top left and right panels present the mixture density (kg m^{-3}) and relative velocity (m s^{-1}), respectively while the bottom left and right panels show the mixture velocity (m s^{-1}) and pressure (Pa), respectively.

In many applications concerning this test case, the Zuber-Findlay law (40) is used in the context of relevant industrial applications of the drift flux model which is a two-fluid model type (Faille and Heintze 1999, Fjelde and Karlsen 2002, Evje and Flatten 2007, Guillard and Duval 2007). The interest of this

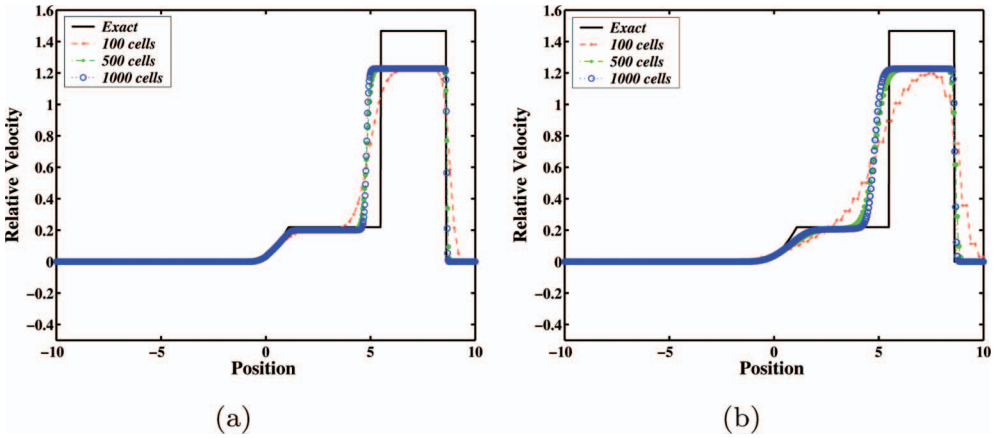

Figure 9. Grid convergence study for the sonic rarefaction test case. Results for the relative velocity (m s^{-1}) profile: exact (solid line) and computed (line with circles, line with points and line with plus signs, respectively) at a time $t = 1$ with CFL = 0.9. The left panel, (a), shows results for the Godunov first-order scheme while the right panel, (b), refers to the Lax-Friedrichs scheme results, respectively.

test case, therefore, lies in applying it to two-phase gas–liquid mixture models with a relative velocity being taken into account. The profiles of the mixture density, relative velocity, mixture velocity and pressure at a time $t = 0.02$ are given in Figure 10(a)–(d). The results show a left propagating shock wave and a right propagating shock wave. Between the left and right shock waves is the star region with constant mixture density and mixture velocity and with a discontinuous relative velocity between the two phases. As displayed in Figure 10(a)–(d), the numerical results obtained using upwind methods compare favourably with exact solutions. Further, all discontinuities of the mixture are well captured and there are no signs of any oscillations.

It is interesting to note that the star region, see Figure 10(a)–(d), differs slightly between the numerical results and the exact solutions in all profiles even with the slip law configuration. As mentioned previously, this is due to the first order of u_r within the exact solver and the second order of u_r in the fluxes used in the numerical methods. In order to elucidate this fundamental issue, we compute the solution for the relative velocity profile at the grid convergence study. The results are presented in Figure 11(a,b). These results are obtained using the Godunov first-order scheme and the Lax-Friedrichs scheme. It is worth underlining that refining the grids for first-order methods cannot eliminate the effect of the relative velocity order on the wave structure.

This test case demonstrates that both the exact solver and the upwind methods can represent propagating discontinuities in two-phase gas–liquid mixture with the Zuber-Findlay law.

5.2.2. *Dispersed law*

This test case is an extension of the dispersed law presented by Baudin *et al.* (2005a) for the drift flux model with the following hydrodynamic law

$$u_r = \frac{-\delta}{1-\alpha}, \quad \text{with} \quad \delta = 1.53 \sqrt[4]{\frac{g\sigma}{\rho_1}}\, sin\theta, \tag{41}$$

where $\sigma = 7.5\ 10^{-5}$ is the superficial stress, g is the gravity and $\theta = \frac{\pi}{2}$.

The left and right states for this Riemann problem are (Baudin *et al.* 2005a)

$$\rho_L = 901.11, \quad u_L = 0.95027 \quad \text{and} \quad \rho_R = 208.88, \quad u_R = 0.78548.$$

It is worth noting that the hydrodynamic law (41) describes small gas bubbles that are dispersed in liquid within an inclined pipe. Further, the above dispersed law has been the subject of extensive and intensive research for the drift flux model in the context of industrial applications of interest. See for example Bendiksen (1984) and Flatten and Munkejord (2006).

Figure 12(a)–(d) displays the behaviour of the solution using Equation (41) for two–phase gas–liquid mixture. Profiles are plotted for the mixture density, relative velocity, mixture velocity and pressure at a time $t = 3$. The solution consists of a left rarefaction wave, a right shock wave and a right travelling contact discontinuity. In addition to that, a surprising feature of this test case for the model at hand is that a left sonic rarefaction wave occurs within the wave structure as demonstrated in Figure 12(a)–(d). It can be observed from Figure 12(a)–(d) that both the numerical and exact results are in excellent agreement. In particular,

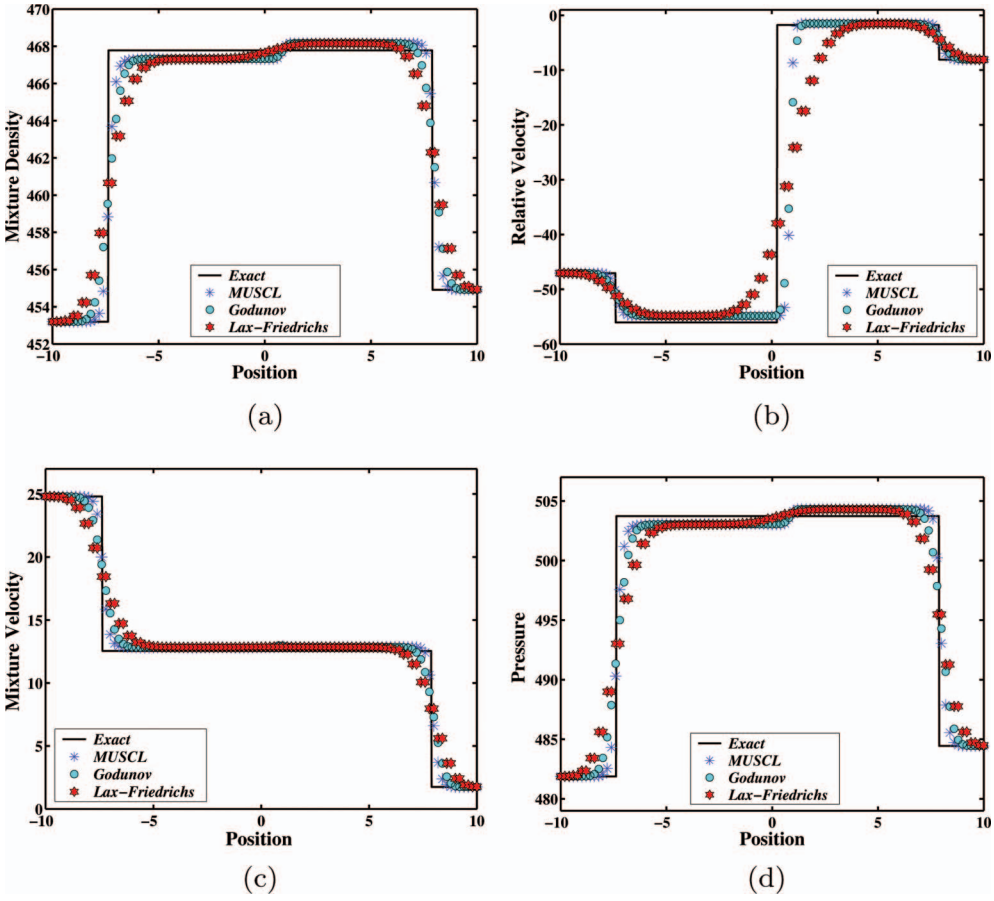

Figure 10. Zuber-Findlay law, test case 5.2.1, of Baudin *et al.* (2005a) which represents the relative velocity law (Zuber and Findlay 1965) within two-phase gas–liquid mixture. Exact solution (solid line) and numerical solutions (symbols) at a time $t = 0.02$ of the Riemann problem with left and right states are given in section 5.2.1 and with the relative velocity given by Equation (40). The solution comprises a left shock wave and a right shock wave separated by a contact discontinuity. Results are shown for the mixture density (kg m^{-3}, top left), relative velocity (m s^{-1}, top right), mixture velocity (m s^{-1}, bottom left) and pressure (Pa, bottom right).

no spurious oscillations can be seen in any of the profiles across the contact wave. Furthermore, the effect of the first and second order in u_r is clearly visible in all the plots of the flow variables, as it should be. By way of further investigation on this consequence, a grid convergence study for both the Godunov first-order scheme and the Lax-Friedrichs scheme is performed as demonstrated in Figure 13(a,b). It can be seen that during the solution at the finest resolution (shown in blue), both methods produce similar results as the exact solution.

5.2.3. *Left shock and right rarefaction*

This test case is designed to verify the ability of the Riemann solver described in section 3 in dealing with known values for the relative velocity as two different states. The initial conditions for this Riemann problem are

$$(\rho, u, u_r)_{\mathrm{L}} = (500\ \mathrm{kg/m^3},\ 0.1\ \mathrm{m/s},\quad 7\ \mathrm{m/s}),$$
$$(\rho, u, u_r)_{\mathrm{R}} = (600\ \mathrm{kg/m^3},\ 1.0\ \mathrm{m/s},\ 8.5\ \mathrm{m/s}).$$

Figure 14(a)–(d) illustrates the solution of this Riemann problem. It is observed that the solution is composed of a left shock and a right rarefaction separated by a contact discontinuity. The exact solution and numerical results computed with the Godunov first-order upwind scheme and the MUSCL-Hancock approach are plotted at a time $t = 0.15$ in Figure 14(a)–(d). In this figure, the gas–liquid mixture wave pattern consists of a left shock and a right rarefaction separated by a contact discontinuity. It is also clear from these plots that upwind methods present similar resolutions as the exact solution, but differ in their ability to resolve the contact discontinuity. As before, the star regions differs slightly between the numerical results and

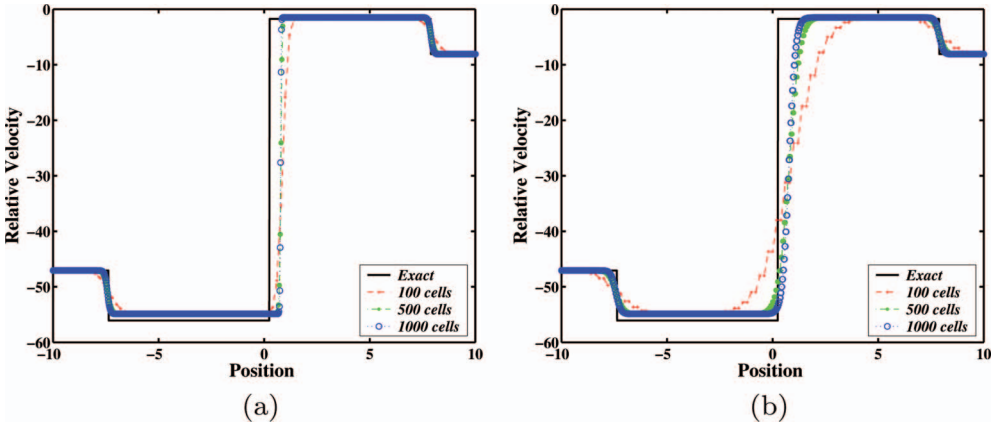

Figure 11. Grid convergence study for the Zuber-Findlay law, test case 5.2.1, of Baudin *et al.* (2005a). Results for the relative velocity (m s^{-1}) profile: computed (line symbols) and exact (solid line with no symbols) at a time $t = 0.02$ with CFL = 0.9. The left panel, (a), displays results for the Godunov first-order scheme while the right panel, (b), represents the Lax-Friedrichs scheme results, respectively.

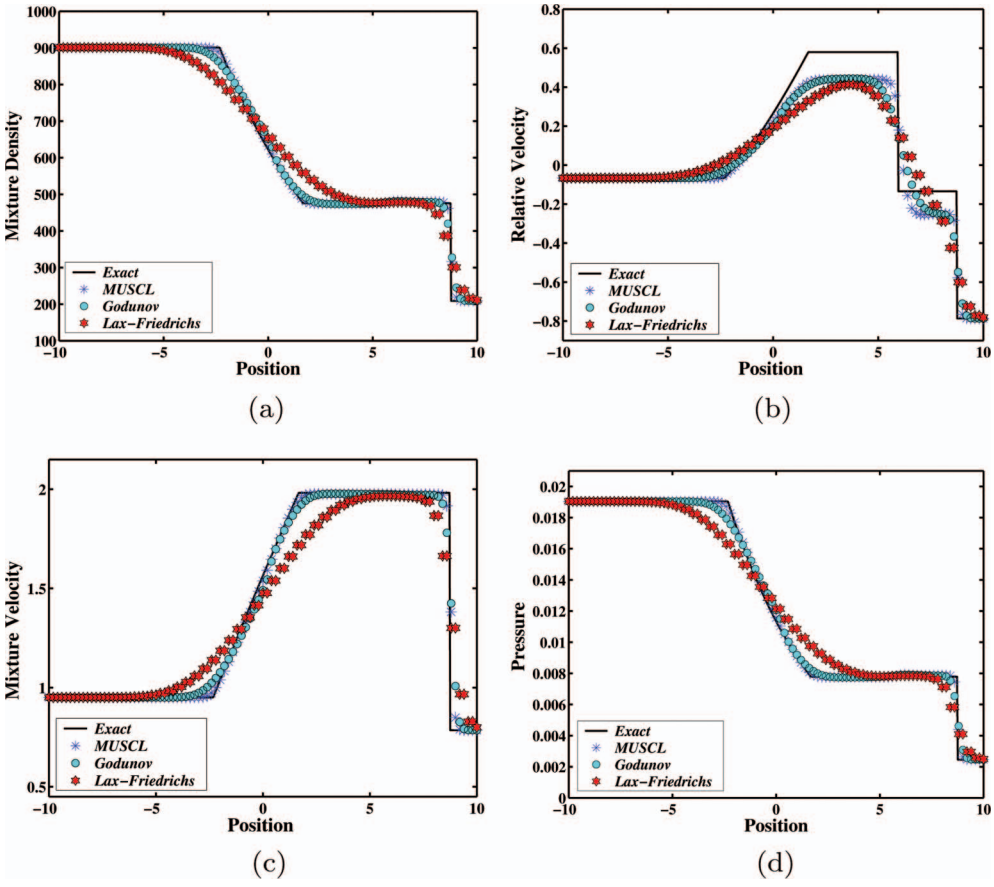

Figure 12. Dispersed law, test case 5.2.2, of Baudin *et al.* (2005a) which represents the relative velocity between the two-phase gas–liquid mixture given in Equation (41). Exact solution (solid line) and numerical solutions (symbols) at a time $t = 3$ of the Riemann problem with left and right states are given in section 5.2.2. The solution is composed of a right going shock wave, a right travelling contact discontinuity and a left sonic rarefaction wave. From top to bottom, left to right, the panels show the mixture density (kg m^{-3}), relative velocity (m s^{-1}), mixture velocity (m s^{-1}) and pressure (Pa).

the exact solutions. This is caused by the order of u_r in the exact Riemann solver and the numerical methods. To see the quantitative information of the solutions, Figure 15(a,b) displays grid convergence study of the relative velocity using the Godunov first-order scheme and the Lax-Friedrichs

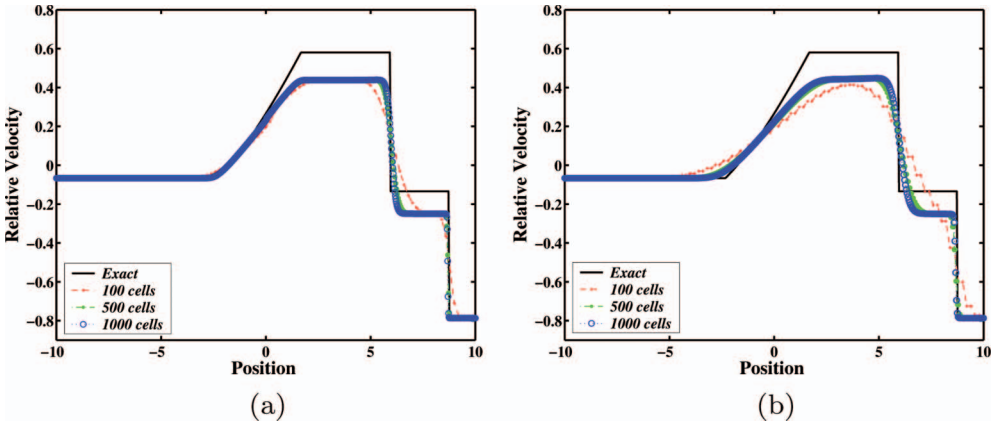

Figure 13. Grid convergence study for the dispersed law, test case 5.2.2, of Baudin *et al.* (2005a). Results for the relative velocity (m s^{-1}) profile: computed (line symbols) and exact (solid line) at a time $t = 3$ with CFL = 0.9. (a) The Godunov first-order scheme resolutions. (b) The Lax-Friedrichs scheme resolutions.

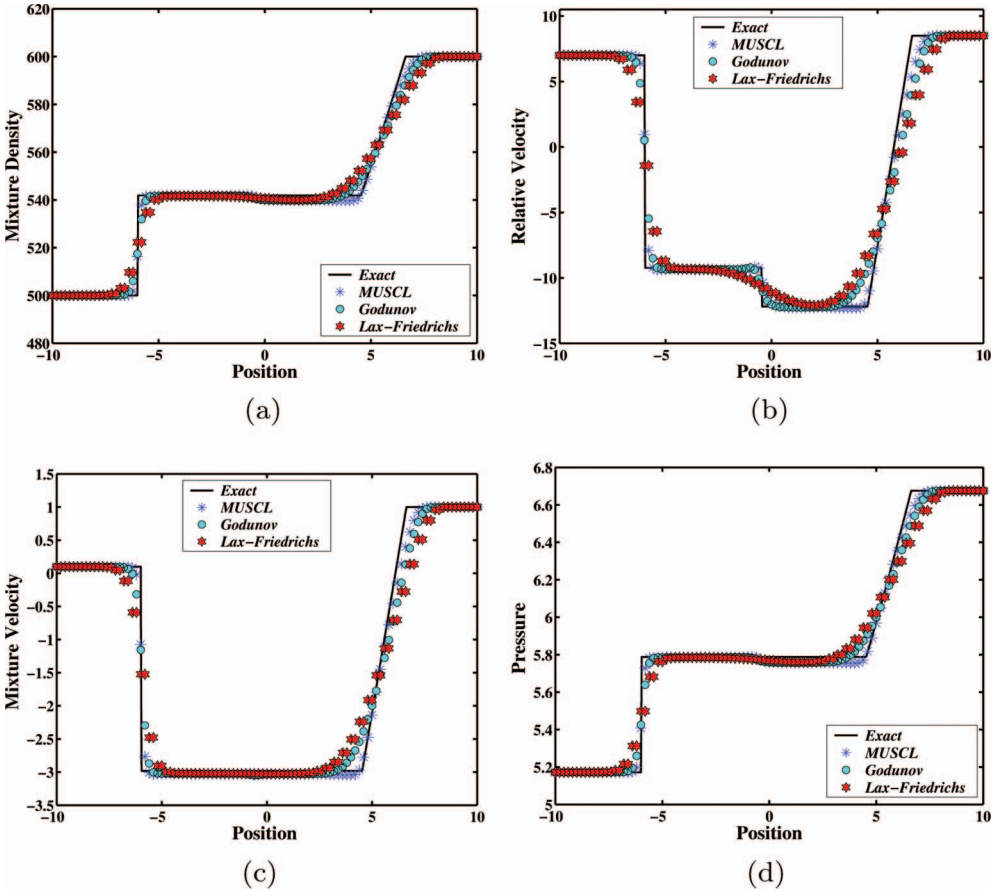

Figure 14. Slip condition test case 5.2.3: left shock wave and right rarefaction wave. Comparison of the exact (solid line) and numerical (symbols) solutions at a time $t = 0.15$ of the Riemann problem with left and right states given in section 5.2.3. The solution is composed of a left going shock wave and a right going rarefaction wave separated by a contact discontinuity. Results are shown for the mixture density (kg m^{-3}, top left), relative velocity (m s^{-1}, top right), mixture velocity (m s^{-1}, bottom left) and pressure (Pa, bottom right).

scheme. From the figure, it is easy to observe the convergence of the methods towards the exact solution for various grid resolutions (shown in red, green and blue). The close agreement between the exact solution and finest resolution are also seen.

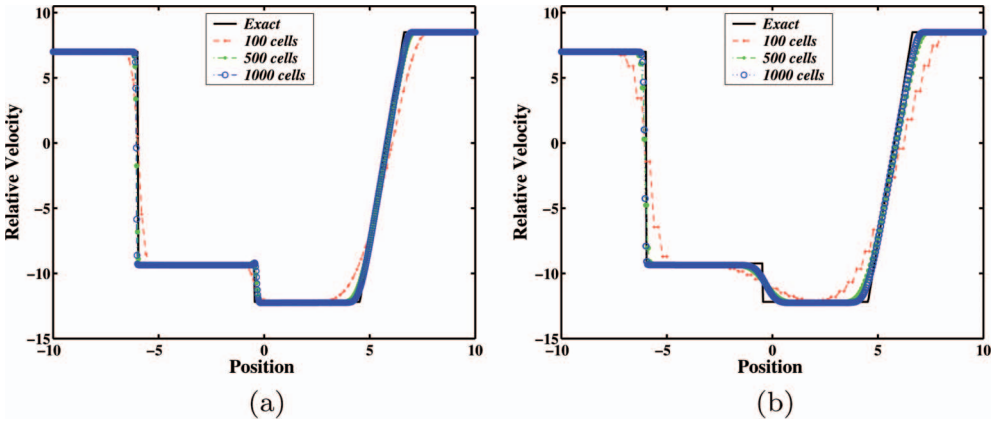

Figure 15. Grid convergence study for the slip condition test case 5.2.3: left shock wave and right rarefaction wave. Results for the relative velocity (m s^{-1}) profile: exact (solid line) and computed (line with circles, line with points and line with plus signs, respectively) at a time $t = 0.15$ with CFL = 0.9. Note that these two results coincide. The left panel, (a), shows results for the Godunov first-order scheme while the right panel, (b), refers to the Lax-Friedrichs scheme results, respectively.

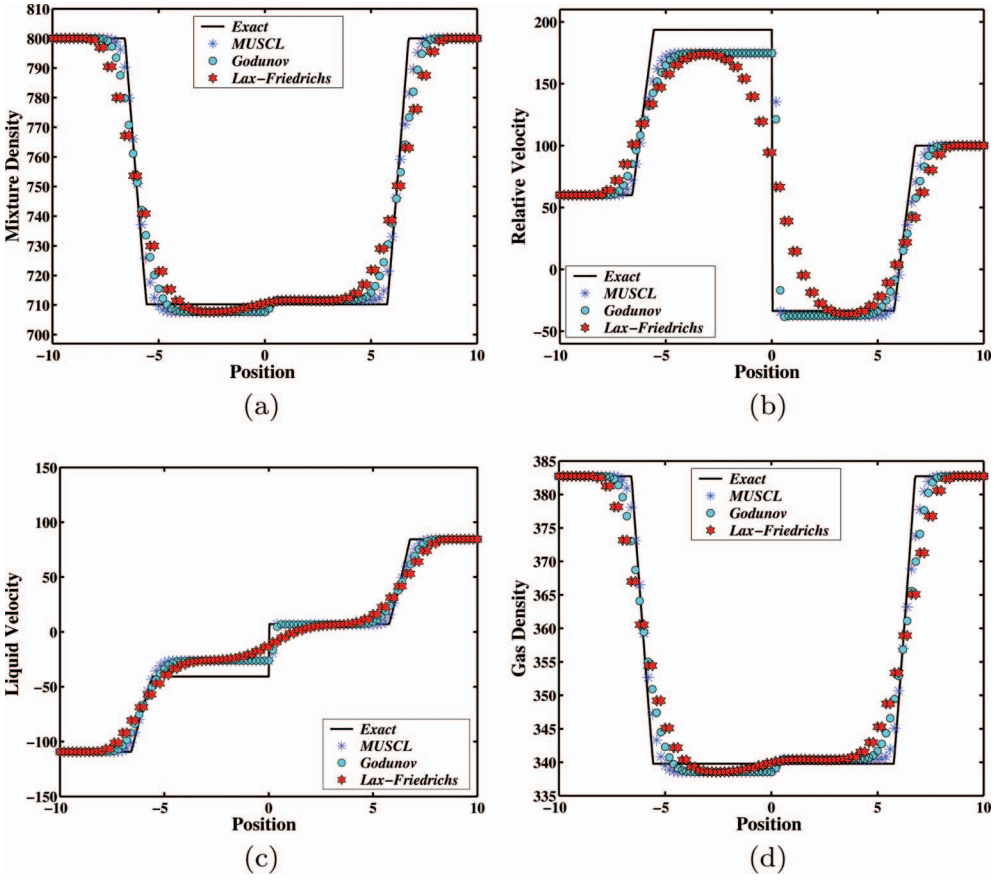

Figure 16. Slip condition test case 5.2.4: left and right rarefaction waves. Comparison of the exact (solid line) and numerical (symbols) solutions of the Riemann problem at a time $t = 0.007$ with left and right states given in section 5.2.4. The solution comprises a left going rarefaction wave and a right going rarefaction wave separated by a contact discontinuity. The upper panels, from left to right refer to the mixture density (kg m^{-3}) and relative velocity (m s^{-1}), respectively while the lower panels, from left to right represent the liquid velocity (m s^{-1}), and gas density (kg m^{-3}).

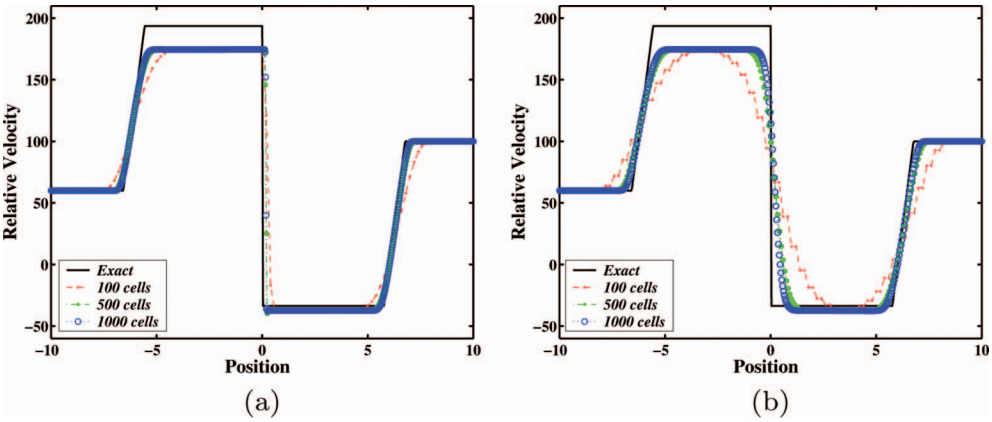

Figure 17. Grid convergence study for the slip condition test case 5.2.4: left and right rarefaction waves. Results for the relative velocity (m s^{-1}) profile: exact (solid line with no symbols) and computed (line with circles, line with points and line with plus signs, respectively) at a time $t = 0.007$ with CFL = 0.9. (a) Refers to the Godunov first-order scheme results. (b) Displays the Lax-Friedrichs scheme results.

5.2.4. *Left rarefaction and right rarefaction*

This test case is performed to assess the performance of the proposed Riemann solver in resolving the left and right waves with two different relative velocity states. In this test case, the initial conditions are defined as

$$(\rho, u, u_r)_{\mathrm{L}} = (800\ \mathrm{kg/m^3}, -100\ \mathrm{m/s},\ 60\ \mathrm{m/s}),$$
$$(\rho, u, u_r)_{\mathrm{R}} = (800\ \mathrm{kg/m^3},\ \ 100\ \mathrm{m/s},\ 100\ \mathrm{m/s}).$$

The initial discontinuity evolves into left and right propagating rarefaction waves with a contact discontinuity in the middle. In Figure 16(a)–(d) the results at a time $t = 0.007$ are displayed and compared with solutions provided by the exact Riemann solver of section 3. The numerical results are computed by the Godunov first-order upwind scheme and the MUSCL-Hancock approach. As one can see, the solutions are oscillation-free for all variables and well reproduce the exact solution. In particular the smooth rarefaction waves are equally resolved by both methods. As it also appears from the plots, the star regions of all the variables differ slightly between the numerical results and the exact solutions. We remind the reader again that this is related to the order of the relative velocity used within the exact Riemann solver and the numerical methods. In order to judge this claim for this test case, we perform a grid convergence study using the Godunov first-order scheme and the Lax-Friedrichs scheme with 100 (shown in red), 500 (shown in green) and 1000 (shown in blue) cells. Of particular interest for this test case, and for the present study, is the relative velocity profile for the two-phase gas–liquid mixture. Figure 17(a,b) displays the results for that at a time $t = 0.007$. One sees immediately that both methods produce similar results as the exact solution at the coarsest and finest resolutions. As it appears from these plots, the numerical resolution is very satisfactory indicating convergence as the grid is refined. Finally, the plots of Figure 17(a,b) gives us confidence that the relative velocity order has given rise to a difference within the wave structure in the star region.

6. Conclusions and future work

The solution of the Riemann problem for solving a hyperbolic two-phase flow model in conservative form has been introduced, developed and studied in this article. A thorough investigation of the features of the model equations allowed us to show that the solution of the Riemann problem can be represented as a set of elementary waves such as shock, contact and rarefaction waves. In this way, a comprehensive mathematical description of the solution in the star region and within the rarefaction waves has been provided. These analyses allowed us to obtain a clear and direct characterisation of the features of both the rarefaction and middle waves. In particular, this middle wave results in a contact discontinuity that divides the star region into two parts and determines the jump conditions in the states across it. These jump conditions agree with earlier investigations presented by Zeidan and Slaouti (2009). We have also successfully used the exact Riemann solver in the development of standard upwind Godunov methods namely the Godunov first-order upwind scheme and the MUSCL-Hancock scheme. The main use of the solver is in the computation of numerical fluxes within these methods. We also conducted a series of numerical test cases by using these methods. The provided results reveal that

the relative velocity effects are specifically associated with theoretical development.

From a numerical point of view, the comparisons between the numerical results and exact solutions show that the model at hand and the solver can handle a variety of demanding problems in two-phase gas–liquid mixture. The excellent agreements obtained in this study can be explained by the fact that the two-phase mixture formulation yields a system of equations that is fully conservative and hyperbolic with a set of eigenvalues and eigenvectors that are all real. The numerical results also show that the effect of the relative velocity, u_r, order between the exact and numerical solutions throughout the star region. This is confirmed by numerical experiments. Furthermore, these experiments set a course for an exciting frontier and may shed new light on our understanding of two-phase gas–liquid mixtures.

This work represents a major advance in the study of wave propagation in two-phase gas–liquid mixture. The theoretical and numerical framework for solving the model equations have been achieved in a one-dimensional context. Thus, further development in both the theoretical and numerical levels is needed for studies involving non-isentropic two-phase flows in one and multiple dimensions. Moreover, further studies combining the proposed exact Riemann solver with other upwind Godunov methods should shed more light on the mathematical and numerical analysis of two-phase fluid flow problems. These topics will be the subject of a future work.

Acknowledgements

The author would like to thank the journal's anonymous reviewers for their helpful comments and suggestions on an earlier version of this article.

References

Andrianov, N., and Warnecke, G., 2004. The Riemann problem for the Baer-Nunziato two-phase flow model. *Journal of Computational Physics*, 195, 434–464.

Baer, M., and Nunziato, J., 1986. A two-phase mixture theory for the deflagration-to-detonation transition (DDT) in reactive granular materials. *International Journal of Multiphase Flow*, 12, 861–889.

Baudin, M., *et al*., 2005a. A relaxation method for two-phase flow models with hydrodynamic closure law. *Numerische Mathematik*, 99, 411–440.

Baudin, M., *et al*., 2005b. A semi-implicit relaxation scheme for modeling two-phase flow in a pipeline. *SIAM Journal on Scientific Computing*, 27, 914–936.

Bendiksen, K.H., 1984. An experimental investigation of the motion of long bubbles in inclined tubes. *International Journal of Multiphase Flow*, 10, 467–483.

Castro, C.E., and Toro, E.F., 2006. A Riemann solver and upwind methods for a two-phase flow model in non-conservative form. *International Journal of Numerical Methods in Fluids*, 50, 275–307.

Deledicque, V., and Papalexandris, M. V., 2007. An exact Riemann solver for compressible two-phase flow models containing non-conservative products. *Journal of Computational Physics*, 222, 217–245.

Drew, D., and Passman, S., 1998. *Theory of multicomponent fluids*. *Applied mathematical sciences*. Vol. 135. New York: Springer-Verlag.

Enwald, H., Peirano, E., and Almstedt, A.-E., 1996. Eulerian two-phase flow theory applied to fluidization. *International Journal of Multiphase Flow*, 22, 21–66.

Evje, S., and Flatten, T., 2007. On the wave structure of two-phase flow models. *SIAM Journal on Applied Mathematics*, 67, 487–511.

Faille, I., and Heintze, E., 1999. A rough finite volume scheme for modeling two-phase flow in a pipeline. *Computers & Fluids*, 28, 213–241.

Flatten, T., and Munkejord, S.T., 2006. The approximate Riemann solver of Roe applied to a drift-flux two-phase flow model. *ESAIM: Mathematical Modelling and Numerical Analysis*, 40, 735–764.

Fjelde, K.K., and Karlsen, K.H., 2002. High-resolution hybrid primitive-conservative upwind schemes for the drift flux model. *Computers & Fluids*, 31, 335–367.

Godunov, S.K., 1959. A difference method for numerical calculation of discontinuous solutions of the equations of hydrodynamics. *Matematicheskii Sbornik*, 47, 357–393.

Gonthier, K.A., and Powers, J., 2000. A high-resolution method for a two-phase model of deflagration-to-detonation transition. *Journal of Computational Physics*, 163, 376–433.

Guillard, H., and Duval, F., 2007. A Darcy law for the drift velocity in a two-phase flow model. *Journal of Computational Physics*, 224, 288–313.

Ishii, M., 1975. *Thermo-fluid dynamic theory of two-phase flow*. Paris: Eyrolles.

LeVeque, R., 1992. *Numerical methods for conservation laws*. Basel: Birkhäuser Verlag.

Luke, E.A., and Cinnella, P., 2007. Numerical simulations of mixtures of fluids using upwind algorithms. *Computers & Fluids*, 36, 1547–1566.

Munkejord, S.T., *et al*., 2006. The multi-stage centred-scheme approach applied to a drift-flux two-phase flow model. *International Journal of Numerical Methods in Fluids*, 52, 679–705.

Sachdev, J.S., Groth, C.P.T., and Gottlieb, J.J., 2007. Numerical solution scheme for inert, disperse, and dilute gas-particle flows. *International Journal of Multiphase Flow*, 33, 282–299.

Saurel, R., and Abgrall, R., 1999. A multiphase Godunov method for compressible multifluid and multiphase flows. *Journal of Computational Physics*, 150, 425–467.

Schwendeman, D.W., Wahle, C.W., and Kapila, A.K., 2006. The Riemann problem and a high-resolution Godunov method for a model of compressible two-phase flow. *Journal of Computational Physics*, 212, 490–526.

Stadtke, H., 2006. *Gas dynamic aspects of two-phase flow: hyperbolicity, wave propagation phenomena, and related numerical methods*. Weinheim: Wiley-VCH.

Stewart, H.B., and Wendroff, B., 1984. Two-phase flow: models and methods. *Journal of Computational Physics*, 56, 363–409.

Toro, E.F., 2009. Riemann solvers and numerical methods for fluid dynamics. *A practical introduction*. Berlin, Heidelberg: Springer-Verlag.

van Leer, B., 1979. Towards the ultimate conservative difference scheme. V. A second-order sequel to Godunov's method, *Journal of Computational Physics*, 32, 101–136.

Zeidan, D., 2011. Numerical resolution for a compressible two-phase flow model based on the theory of thermodynamically compatible systems. *Applied Mathematics and Computation*, 217, 5023–5040.

Zeidan, D., and Slaouti, A., 2009. Validation of hyperbolic model for two-phase flow in conservative form. *International Journal of Computational Fluid Dynamics*, 23, 623–641.

Zuber, N., and Findlay, J., 1965. Average volumetric concentration in two-phase flow systems. *ASME Journal of Heat Transfer*, 87, 453–458.

Zeidan, D., *et al.*, 2007. Numerical study of wave propagation in compressible two-phase flow. *International Journal of Numerical Methods in Fluids*, 54, 393–417.